Gating motions in voltage-gated potassium channels revealed by coarse-grained molecular dynamics simulations

Treptow, W.; Marrink, S.J.; Tarek, M.

Published in:
Journal of Physical Chemistry B.

DOI:
10.1021/jp709675e

Publication date:
2008

Gating motions in voltage-gated potassium channels revealed by coarse-grained molecular dynamics simulations

Werner Treptow[‡], Siewert-J Marrink,[†] and Mounir Tarek[*]

METHODS

Coarse-Grain (CG) modelling of peptide-lipid systems

i.1) Basic Coarse-Grain (CG) parameters: The basic parameters for the combined peptide-lipid force field are the same as used for the lipid force field described previously [1]. It uses a four-to-one mapping, i.e. on average four heavy atoms are represented by a single interaction center. Currently the model considers four main types of interaction sites only: polar (P), non-polar (N), apolar (C), and charged (Q). For particles of type N and Q four subtypes (0, *d*, *a*, and *da*) are further distinguished. Subtype 0 applies to groups in which no hydrogen bonding capabilities exist, *d* and *a* for groups that could act as a hydrogen bond donor or acceptor, respectively, and *da* for groups with both donor and acceptor options. All non-bonded particles interact via a Lennard-Jones (LJ) potential. The strength of the interaction, determined by the value of the well-depth ε_{ij}, depends on particle type *i* and *j*. The value of ε ranges from ε=5 kJ/mol for interactions between polar groups to ε =1.8 kJ/mol for interactions between polar and apolar groups mimicking the hydrophobic effect. The effective size of the particles is governed by the LJ parameter σ = 0.47 nm for all particle types. For reasons of computational efficiency a mass of *m* = 72 amu (corresponding to four water molecules) is assigned to each CG site. In addition to the LJ interaction, charged groups (type Q) interact via the normal electrostatic *Coulombic* potential applying a relative dielectric constant ε_{ij} =20 for explicit screening.

Bonded interactions between chemically connected sites are described by a weak harmonic potential with an equilibrium distance $R_{bond} = \sigma = 0.47$ nm, and a force constant of $K_{bond} = 1250$ kJ.mol^{-1}.nm^{-2}. To represent chain-stiffness, a weak harmonic potential is used for the angles with equilibrium bond angle $\theta_0 = 180^0$, with a force constant of $K_{angle} = 25$ kJ mol^{-1}rad^{-2}. More details about the CG lipid model can be found in the original paper [1].

i.2) Parametrization for peptides: Most amino acids were mapped onto single standard particle types in a similar way as was done recently by other groups [3,4]. The most apolar amino acids (Leu, Pro, Ile, and Val) were represented as C type particles, intermediately polar amino acids by N*da* (Ser, Thr) or N0 (Met, Cys), the polar uncharged amino acids by P (Asn, Gln), and the charged side chains as Q*d* (Lys), Q*a* (Glu, Asp), or Q*da* [5 5]. The larger Arg side chain was modeled by two particles (N*d*-Q*da*), and the bulkier ring-based side chains by three N0-N0-N0 [6], N0-N0-N*da* (Tyr), or C-C-N*d* (Trp) CG particles. The Gly and Ala residues were only represented by the backbone particle, which is in general of type N0 for all residues. Hence, main-chain beads along the TM regions were defined as non-polar (N0 type) whereas those in the water-exposed regions received a polar characteristic (P type) to ensure the correct partitioning of channel segments through the water/lipid environment. Note that inadvertedly, the bead types for Thr and Cys were swapped in the actual simulations. In Kv1.2 these residues are mostly located in the hydrated loops of the channel, and the poor representation of theses residues is therefore unlikely to affect the major finding of the paper. Finally, histidine residues considered in the present study were charged.

The particle types for most amino acids were estimated from a comparison between simulation results and experimental measurements of the water/oil partitioning coefficients of the amino acid side chain analogues. In the actual version of the force field, the experimental values could be reproduced to within 2 kT for most. The assignment of particle types and the partitioning behavior is summarized in Table 3.

The geometry of the amino acids in the peptide force field is such as to mimic the underlying chemical structure as closely as possible (cf. Table 3). One important feature of this force field is that bond lengths are allowed to deviate from the standard value of 0.47 nm as defined in the lipid force field. The current force field is not able to spontaneously fold peptides into helices, so two constraints are necessary: 1) a 90 degrees angle constraint between three sequential backbone sites (K=1250), and 2) a 1-5 distant constraint at 0.60 nm (K=12500 kJ.mol^{-1}.nm^{-2}).

TABLE 3 Structure and Partitioning free energies (in kJ/mol) between water and oil for amino acids side chains in the CG model.

Residue	Bead type	Geometry[%]	ΔG^{CG}	ΔG^{Exp}
Leu	C	2.6 (12.5)	22	22
Ile	C	2.3 (5.0)	22	22
Val	C	1.5 (12.5)	22	17
Pro	C	1.8 (12.5)	22	-
Met	NO	4.1(1.25)	12	10
Cys	NO	2.8 (12.5)	12	5
Thr	N*da*	1.8 (12.5)	-12	-11
Ser	N*da*	1.5 (12.5)	-12	-14
Gln	P	3.4 (5.0)	-23	-25
Asn	P	2.6 (12.5)	-23	-28
His	Q*da*	3.4 (5.0)	-23	-
Lys	Q*d*	4.0 (1.25)	-23	-
Asp	Q*a*	2.6 (12.5)	-23	-
Glu	Q*a*	3.8 (5.0)	-23	-
Arg	N*d*-Q*da*	3.0-2.5 (1.25,5.0) 180 (0.025)	< -25	-
Phe	NO-NO-NO	3.3-3.3-4.5 (3x12.5) 1.5-1.5-1.5 (3x12.5) 30-30 (2x1.25)	19	17
Trp	N*d*-C-C	3.4-5.65- -(2x12.5) 2.9-2.9-1.5 (3x12.5) 127-97 (2x0.25)	20	9
Tyr	N*da*-NO-NO	3.5-3.5-5.5 (3x12.5) 1.5-2.2-2.2 (3x12.5) 20-20 (2x1.25)	2	-2

Simulation data are calculated from equilibrium densities of low concentrations of CG beads dissolved in a water/butane two phase system. The experimental data are taken from [7,8] and refer to partitioning between water and cyclohexane. Both the simulation and the experimental data are obtained at 300K. [%] The geometry of the side chains are listed as follow: For one bead components: the backbone to side chain bond equilibrium distances and corresponding force constants (10^3 kJ.mol^{-1}.nm^{-2}) (between brackets). For side chains of beads 2-3-4 (1 being the backbone bead) are given the equilibrium distances (1-2,1-3,1-4,2-3,2-4 and 3-4) and the corresponding force constants, as well as the equilibrium angles and the corresponding force constants (10^3 kJ mol^{-1}rad^{-2}).

The current set-up has been tested on the behavior of small peptides with respect to membrane binding. It was found that the preferred binding mode, i.e. whether interfacially bound or in a TM orientation, for a series of α-helical peptides could be well reproduced. Although this initial set-up as well as similar ones [3,4] seems to behave quite realistically, a more thorough design and testing of the protein CG force field is currently underway and will be published elsewhere.

Although the variables of the CG system (densities, length scales, energies, temperature, pressure) keep their physical meaning, this is not strictly true for the time scale. In comparison to atomistic models, the dynamics of the CG model are faster. The main reason is that the underlying energy landscape is much smoother as a result of the larger particle sizes. When interpreting the simulation results with the CG model, one can to a first approximation simply scale the time axis. The standard conversion factor we use is a factor of 4, which is the effective speed up factor in the diffusional dynamics of CG water compared to real water. Somewhat surprisingly, this factor appears to describe the general dynamics present in many membrane systems quite well. For instance, water permeation rates across the membrane and lipid lateral diffusion rates are observed to be in good agreement with experimental measurements [1]. More global events such as the aggregation of lipids into vesicles occurs on a similar time scale when compared to atomistic level models [9]. Likewise, the sampling speed of the configurational space of the lipid tails inside a bilayer was compared between the CG model and an atomistic model [10]. Again, after scaling the CG dynamics by a factor of 4, the results turned out to be very similar. No explicit comparison has been performed for the dynamics of proteins, however, so the effective time scale reported in the main paper should be interpreted with care.

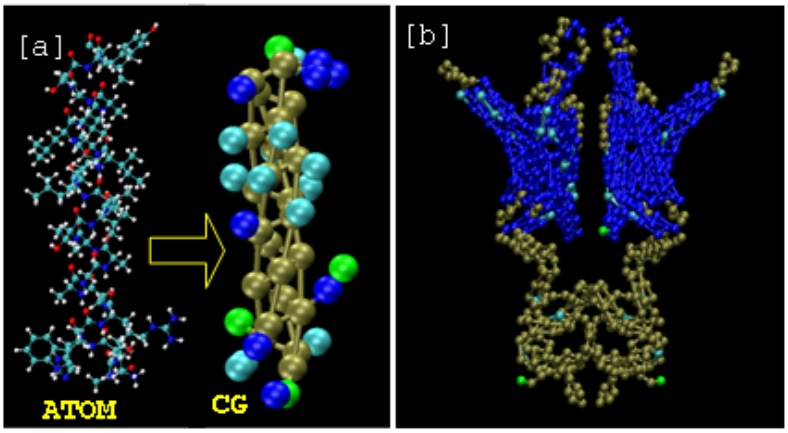

FIGURE 5. Coarse-grain model of Kv channels. [a] Transformation of a full-atomistic helix (left) into a CG one (right). The helical conformation in the CG structure is imposed by main-chain bonds and angle constraints (see text). CG beads are colored by type, *e.g.*, polar (tan), charged (green), non-polar (blue) and apolar (cyan). [b] CG model of the Kv1.2 channel. For clarity, only beads of the main chain are drawn. Note that beads along the TM helices are defined as non-polar whereas those in the water exposed regions (T1 domain and T1-S1 linker and TM loops) have a polar characteristic. This property ensures the correct partitioning of helices through the water/lipid milieu.

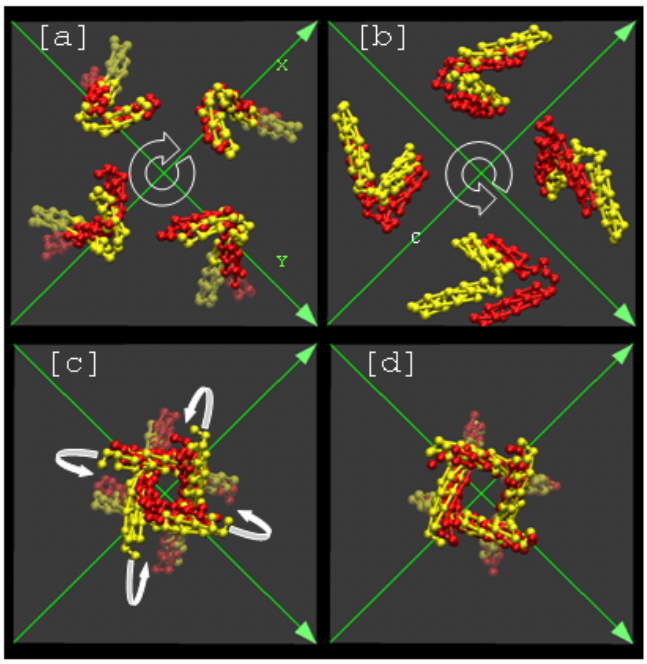

FIGURE 6. Coupled motions in Kv1.2^{TM} [a, c] and KvAP [b, d]. For each channel, conformations at the beginning (yellow) and at the end (red; t=350 ns) of the simulation are compared by means of structural superposition (see Table 1 for rmsd values). Only the main chain of S4 together with the S4-S5 linker [a, b] or S6 [c, d] are drawn (bottom view). For Kv1.2^{TM}, the mechanistic coupling between the voltage-sensor and the pore is similar to that observed in the simulation of the complete channel (see fig. 2). For KvAP, the coupling between S4 and S6 is small in spite of a significant overall rotation of the voltage sensor about the channel main axis (white arrow).

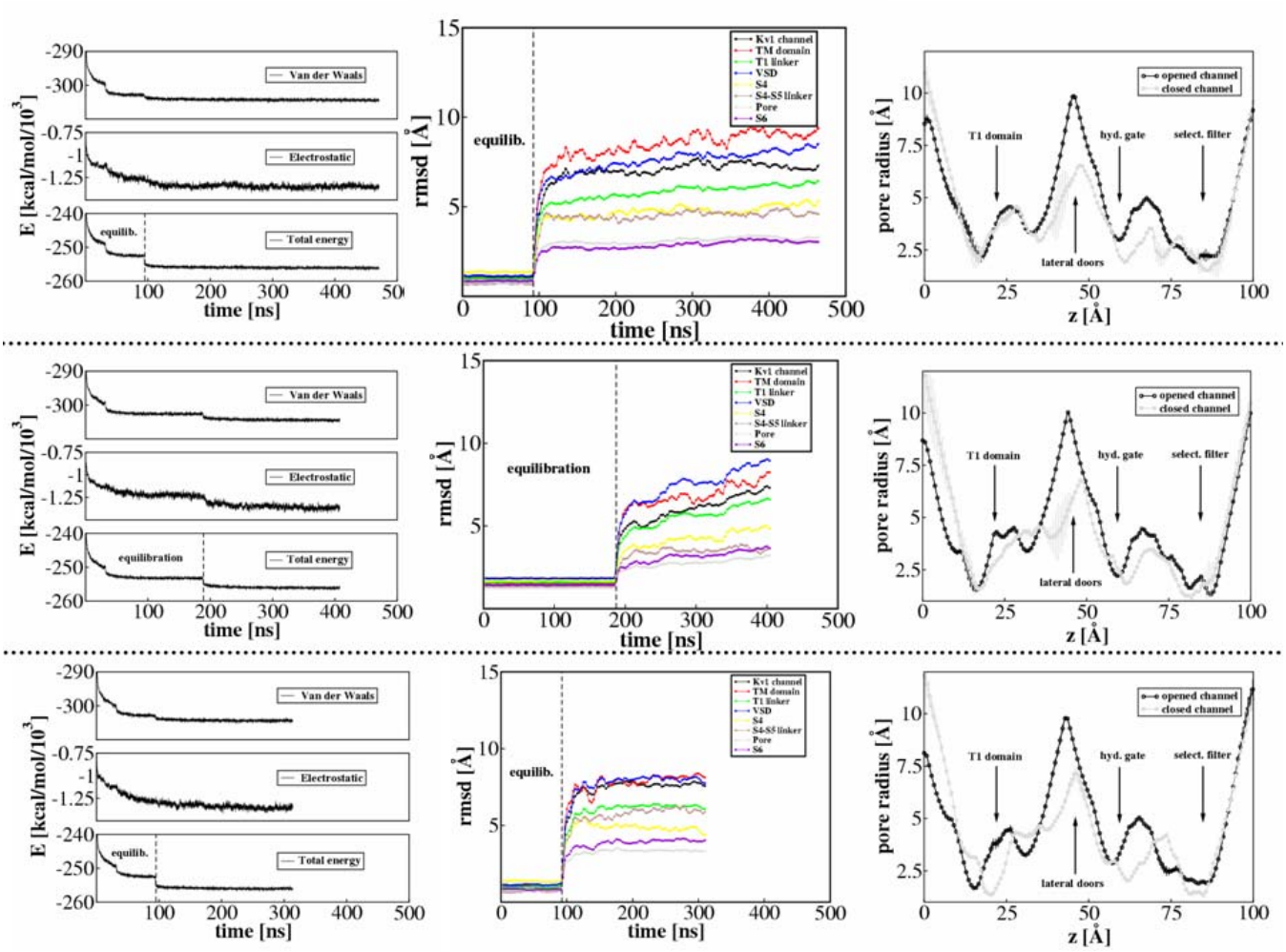

FIGURE 7. Results from three independent simulations of the KV1.2 channel showing from left to right the energies of the system, the rmsd's of the channel fragments with respect to the initial structure, and the pore radius profiles of the open (initial) structure and the final converged structure. In these simulations, different equilibration protocols and different numbers of hydration beads placed initially in the central cavity were considered. The major findings agree with those presented in the main text. The CG structure was constrained during the equilibration stages to allow for full reorganization of the water and lipids. The rmsd's were calculated with respect to the initial coarse grain structure by superposing the beads of the P helices of the tetramer as the later did not deviate from the initial construct. The pore-radius profile for the opened and closed conformations of the Kv1.2 channel measured using Hole.[2] Both profiles are averages calculated over a time window of 30 ns at the beginning (black) and at the end (gray) of the simulation. Average-standard deviations are shown as bars. The profiles span the complete channel, including both the T1 and TM domains. Note that, major changes were found for the lateral doors located at the interface between the T1 and TM domains, for the hydrophobic gate formed by the PVPVIV motif in the pore region and for the central cavity placed between the latter and the selectivity filter.

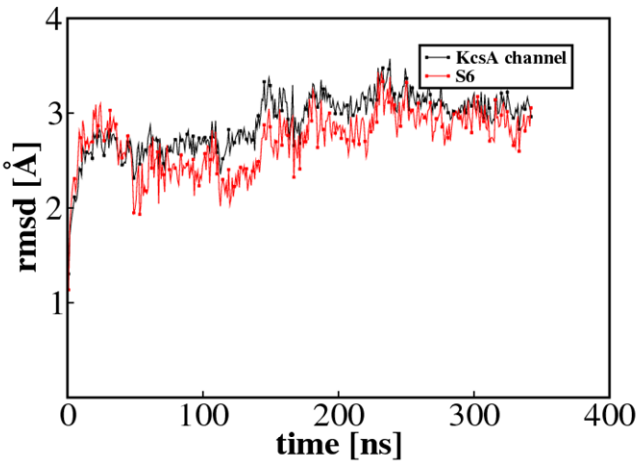

FIGURE 8. Evolution of the rmsd's of the KcsA channel from the initial crystal structure as a function of time along a CG simulation of the channel in a membrane environment. The rmsd's were calculated with respect to the initial coarse grain structure by superposing the beads of the P helices of the tetramer as the later did not deviate from the initial construct.

Movie Caption:

Movie 1: Coarse-grain MD simulation (350 ns) of Kv1.2 channel embedded in the lipid bilayer highlighting the overall conformational rearrangement of the model during the closing process. The lipid (licorice) and the channel (van der Walls) are colored by atom and segment type, respectively. One notes the contraction of cytoplasmic lateral portals due to a peculiar motion of the intracellular tetramerization T1 domain. The upward motion of the latter favors the interaction between residues of the T1-S1 linker (green), residues of the S4-S5 linker and residues in the C terminal of S6. Note that the protein backbone beads are is held fixed during the initial equilibration run.

Movie 2: Conformational changes of the transmembrane region of the Kv1.2 channel from a 350 ns coarse-grain MD simulation. The protein is shown as a C^{α} trace, with S6 drawn in green, S5 in red, S4 in yellow and S1-S3 in blue. The P helices joining S5 and S6 are drawn in white and the S4-S5 linker in orange. Positive residues in S4 (blue), negative residues in S2 and S3 (red) and the hydrophobic gate V^{478} in the pore region (magenta) are also depicted. Finally, lime and cyan beads represent water molecules hydrating the regions of the VS and the pore domain, respectively. In the closing process of the CG model, water is expelled from the VS domain inducing conformational changes of S4 that are further communicated to the hydrophobic gate in the pore region. One notes that S4 motions are accompanied by the rearrangement of salt-bridge interactions in the VS domain. Note that the protein backbone beads are is held fixed during the initial equilibration run.

REFERENCES

(1) Marrink, S. J.; Vries, A. H.; Mark, A. E. *J. Phys. Chem. B* **2004**, *108*, 750.
(2) Smart, O. S.; Goodfellow, J. M.; Wallace, B. A. *Biophys. J.* **1993**, *72*, 1109.
(3) Shih, A. Y.; Arkhipov, A.; Freddolino, P. L.; Schulten, K. *J. Phys. Chem. B* **2006**, *110*, 3674.
(4) Bond, P. J.; Sansom, M. S. P. *J. Am. Chem. Soc.* **2006**, *128*, 2697.
(5) Zhong, Q.; Hisslein, T.; Moore, P. B.; Newns, D. M.; Pattnaik, P.; Klein, M. L. *FEBS Lett.* **1998**, *434*, 265.
(6) Ragsdale, D. S.; McPhee, J. C.; Scheuer, T.; Catterall, W. A. *Proc. Natl. Acad. Sci. USA* **1996**, *93*, 9270.
(7) Radzicka, A.; Wlfenden, R. *Biochemistry* **1988**, *27*, 1664.
(8) Wolfenden, R.; Andersson, L.; Cullis, P. M.; Southgate, C. C. B. *Biochemistry* **1981**, *20*, 849.
(9) Van Der Spoel, D.; Lindahl, E.; Hess, B.; Groenhof, G.; Mark, A. E.; Berendsen, H. J. C. *J. Comp. Chem* **2005**, *26*, 1701.
(10) Baron, R.; de Vries, A. H.; Hunenberger, P. H.; W.F., v. G. *J. Phys. Chem. B* **2006**, *110*, 15602.